# Modal liquid crystal wavefront corrector

**S. P. Kotova, M. Yu. Kvashnin, M. A. Rakhmatulin and O. A. Zayakin,**
*P.N. Lebedev Physical Institute of Russian Academy of Sciences, Samara Branch,*
*221 Novo Sadovaja St., Samara 443011, Russia*

**I. R. Guralnik and N. A. Klimov,**
*Samara State University, Pavlova St. 1, Samara 443011, Russia*

**P. Clark, G. D. Love, A. F. Naumov and C. D. Saunter,**
*University of Durham, Dept. of Physics, South Road, Durham, DH1 3LE, UK*
*g.d.love@durham.ac.uk*

**M. Yu. Loktev and G. V. Vdovin,**
*Electronic Instrumentation, TU Delft, P.O.Box 5031, 2600 GA Delft, The Netherlands*

**L. V. Toporkova**
*Volga-Region National Academy of Information and Telecommunications, L.Tolstogo St. 23, Samara 443010, Russia*

**Abstract:** Results are presented of the properties of a liquid crystal wavefront corrector for adaptive optics. The device is controlled using modal addressing in which case the device behaves more like a continuous facesheet deformable mirror than a segmented one. Furthermore, the width and shape of the influence functions are electrically controllable. We describe the construction of the device, the optical properties, and we show experimental results of low order aberration generation.

**OCIS:** (010.1080) Adaptive optics; (230.6120) Spatial light modulators; (120.5060) Phase modulation; (350.1260) Astronomical optics; (230.2090) Electro-optical devices; (230.4110) Modulators

---

## References and links

1. R. H. Freeman, J. E. Pearson, "Deformable mirrors for all seasons and reasons," Appl. Opt. **21**, 580-588 (1982).
2. G. Vdovin, S. Middlehoek, P.M. Sarro, "Technology and application of micromachined silicon adaptive mirrors," Opt. Eng. **35**, 1382-1390 (1997).
3. C. Paterson, I. Munro, and J.C. Dainty, "A low cost adaptive optics system using a membrane mirror," Opt. Express **6,** 175-185 (2000) http://www.opticsexpress.org/abstract.cfm?URI=OPEX-6-9-175
4. D. Dayton, S.R. Restaino, J. Gonglewski, J. Gallegos, S. McDermott, S. Browne, S. Rogers, M. Vaidyanathan, and M. Shilko. "Laboratory and field demonstration of a low cost membrane mirror adaptive optics system," Opt. Commun**. 176,** 339-345 ( 2000)
5. Gordon D. Love. "Liquid crystal adaptive optics." In *Adaptive Optics Engineering Handbook*, Robert K. Tyson, Ed. (Marcel Dekker Inc, 1999) and references therein.
6. S.R. Restaino, D. Dayton, S. Browne, J. Gonglewski, J. Baker, S. Rogers, S. McDermott, J. Gallegos and M. Shilko, "On the use of dual-frequency nematic material for adaptive optics systems: first results of a closed-loop experiment," Opt. Express **6,** 2-6 (2000). http://www.opticsexpress.org/abstract.cfm?URI=OPEX-4-9-344
7. D. Dayton , S. Browne, J. Gonglewski, and S.R. Restaino. "Characterization and control of a multielement dual-frequency liquid-crystal device for high-speed adaptive optical wave-front correction," Appl. Opt. **40,** 2345-2355 (2001)
8. G.D. Love, "Liquid-crystal phase modulator for unpolarized light," Appl. Opt. **32**, 2222-2223 (1993).
9. Thu-Lan Kelly and Gordon D. Love. "White-light performance of a polarization-independent liquid crystal phase modulator," Appl. Opt. **38,**1986-1989 (1999).
10. Gordon D. Love, "Wavefront correction and production of Zernike modes with a liquid crystal SLM," Appl. Opt. **36,** 1517-1524 (1997).
11. A. F. Naumov "Wavefront correctors based on liquid crystal modulators," *in XVI All-Union Tutorial: Physical Principles of Holography*, "Holography methods in science and technique," Leningrad 216-221 (1985).
12. G. Love, J. Major, and A. Purvis. "Liquid crystal prisms for tip—tilt adaptive optics,'' Opt. Lett. **19,** 1170-1722 (1994).

13. O. A. Zayakin, M. Yu. Loktev, G. D. Love, A. F. Naumov, "Cylindrical adaptive lenses," *in 6th International Symposium on Atmospheric and Ocean Optics*, Proc. SPIE **3983,** 112-117 (1999).
14. G. V. Vdovin, I. R. Guralnik, S. P. Kotova, M. Yu. Loktev, A. F. Naumov, "Liquid crystal lenses with programmable focal distance. Part I: Theory, Part II: Experiment," Quantum Electron. **29,** 256-264 (1999).
15. A. F. Naumov, "Modal wavefront correctors," Proc. P. N. Lebedev Physical Institute **217,** 177-182 (1993).
16. A. F. Naumov, G. V. Vdovin, "Multichannel LC-based wavefront corrector with modal influence functions," Opt. Lett. **23,** 1550-1552 (1998).
17. S. P. Kotova, I. R. Guralnik, M. Yu. Loktev, A. F. Naumov, "Adaptive optics modal LC devices," *in Proceedings of First Asia-Pacific Conference APCOM'2000 (Vladivostok, Russia),*"Fundamental problems of opto- and microelectronics" 183-189 (2000).
18. I. Guralnik, M. Loktev, and A. Naumov, "Modal control principle: a new way to the design of liquid-crystal adaptive optics devices," *in Propagation in the Atmosphere and Adaptive Optics.* Proc. SPIE **4338**, 171-181, 2000.
19. I. R. Guralnik, V. N. Belopukhov, G. D. Love, A. F. Naumov, "Interdependence of the electrical and optical properties of liquid crystals for phase modulation applications," J. Appl. Phys. **87,** 4069-4074 (2000).
20. A.Korn, M. Korn *Mathematical Handbook* (McGraw-Hill, 1968).
21. M.B. Allen, E.I. Isaacson, *Numerical analysis for applied science* (Wiley, New York, 1998).
22. http://www.cyanogen.com/products/quickfringe
23. U. Efron, S. T. Wu, T. D. Bates, "Nematic liquid crystals for spatial light modulator: recent studies," J. Opt. Soc. Am. B **3,** 247-252 (1986).
24. Xilinx Inc., San Jose, Ca. http://www.xilinx.com/
25. X Engineering Software Systems Corp., Apex, NC. http://www.xess.com
26. M. Loktev, G. Vdovin, P.Sarro. "Development of a silicon based modal liquid crystal wavefront corrector," To be published in SPIE (2002)

## 1. Introduction

The aim of this work is the development of low-cost wavefront correctors for adaptive optics which can be used in astronomy, medicine and industry. The wavefront corrector is a basic component in any adaptive optics system, and also it is the part which is the most limiting, in the sense that low cost (~few $K), high performance (hundreds or thousands of actuators) wavefront correctors are not commercially available. Piezoelectric deformable mirrors [1] are the current technology of choice for astronomy, however they are expensive for non-astronomical applications, and it seems unlikely that the technology can be scaled to produce mirrors with ~$10^5$ actuators required for very high order adaptive optics. Even though the device described here has only 37 actuators, the technology can easily be scaled to a very large number of actuators. A number of successful low-cost adaptive optics systems have been produced based on silicon-based membrane mirrors [2,3,4]. These mirrors are never-the-less limited by their small size (which is a problem in astronomy because of the large demagnification factor required) and the fact that they are relatively fragile. An ideal wavefront corrector would be easily scalable both in size, and in the number of actuators. Liquid crystal (LC) wavefront correctors have been proposed as such a technology (see Ref. [5] for a review). The procedure of manufacturing LC wavefront correctors is based on the well developed technology of LC displays. They have number of advantages; *viz.* no hysteresis, low control voltages, low power consumption, high reliability and both reflection and transmission modes. Against these advantages, LCs are limited by their slow response speed, their polarization dependence, and the fact that devices which have a large number of actuators and a large fill factor simultaneously are not commercially available. It is the latter constraint which is the subject of this paper. The other two have been addressed elsewhere [6,7,8,9]. The alternative to LC technology is MEMS technology, which is a relatively undeveloped technology.

A conventional electrically addressed LC is controlled by "pixels" which control the phase over an area governed by the geometrical size of the pixel [10]. The pixels are usually on a square or hexagonal grid. We refer to this type of corrector as a "zonal corrector." Normally smooth phase profiles are required, and the zonal LC has a piston-only influence function, which leads to phase discontinuities between the pixels (they are analogous to a segmented mirror with a piston-only influence function). Therefore a larger number of pixels are required to fit a given wavefront than, for example, a Gaussian influence function of a

deformable mirror. (The influence function in general, is defined as the size and shape of the phase distortion around a contact when a voltage is applied).

Non-pixelated modal LC wave front correctors with continuous phase distributions have been previously described for simple aberrations such as slope [11,12], cylindrical [13] and spherical [14]. They have one or two control channels. The modal approach to LC correctors has been extended for a multichannel systems [15,16,17]. The modal principle in LC correctors is based on the production of a continuous rms voltage profile across the LC layer, which is formed by the distributed resistance of the control electrode, and the distributed capacitance and conductance of the LC [18]. Because the electrical properties of LC depend on a frequency [19] then the shape of the rms voltage distribution depends on the control voltage frequency as well. This makes the influence function width controllable.

Here we present the results of a custom built liquid crystal modal wavefront corrector (LC-MWC). We describe the construction of the device, its optical properties, and show how the device can be used to produce low order wavefront aberrations, using a numerical model of the device.

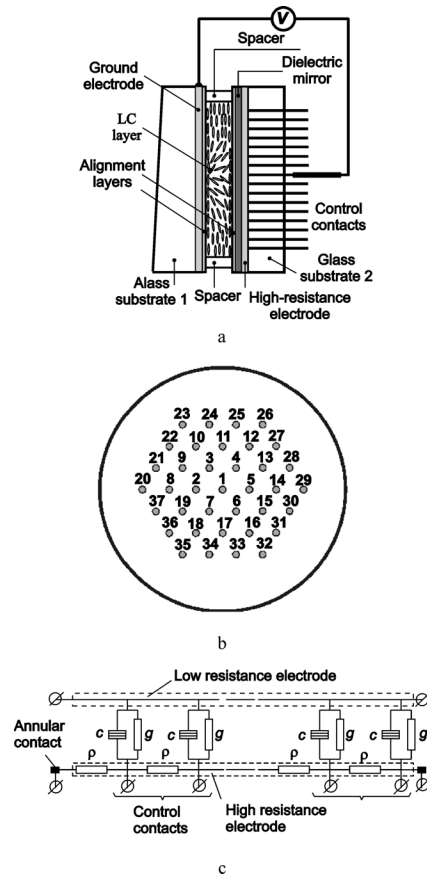## 2. Basic Design and Principle of Operation

Fig. 1. a) Schematic diagram of a multichannel LC wavefront corrector; b) contact arrangement; c) simplified equivalent circuit: $\rho$ is the sheet resistance of the high resistance electrode, $c$ and $g$ denote the capacitance and conductance of the LC layer per unit area. Ø denotes an external electrical connection.

The design of a reflective multichannel LC-MWC and its electrical analog are illustrated in Fig. 1. A layer of nematic LC is sandwiched between two glass substrates coated with transparent electrodes. Calibrated teflon spacers set the thickness of this layer (25µm, therefore the switching speed is slow in this device). The transparent electrode deposited upon the front glass substrate has a low surface resistance and functions as a common electrode. Conversely, the rear electrode is of a much higher resistance (~MΩ/square). The spatial control of the phase in the LC layer is achieved using metal contacts which run through the glass substrate and are connected to the high resistance electrode. The control contacts, of 0.5mm diameter, are arranged in a hexagonal structure with a 3.3mm spacing. A multilayer dielectric reflecting coating, optimised for λ=0.63 µm, is deposited on to the high resistance electrode. The cell alignment is anti-parallel (i.e. the cell operates in the electrically controlled birefringence mode to avoid disclinations which can occur if the cell is parallel aligned). The electric field across the cell at any point where there is a control contact is approximately given by the voltage applied to that contact. In between the contacts the field depends on both the voltage and the frequency of the voltage applied to the neighbouring contacts. If a low frequency field is used, then the field across the cell near to a contact is very similar to the field at the contact. If a higher frequency is used then the field across the cell rapidly falls off away from the point contacts. The field distribution across the cell around a contact is approximately circularly symmetric, and therefore the resultant effect is a wavefront corrector with a controllable influence function: for low frequencies the influence function is broad, and for high frequencies it is narrow. In a deformable mirror the influence function depends on the mechanical properties of the mirror, and it can not be changed once constructed. The mirror can only be controlled by changing the amplitude of the control signal on each actuator. However, in a LC-MWC the optical response can be controlled by the control signal amplitude, frequency, spectral content, and the relative phase between different contact voltages, or a combination of them all.

A mathematical description of the variation of the field across the device proceeds as follows. The sinusoidal voltage across the LC layer at a particular point in the device will have a phase lag with respect to the voltage across the cell at the nearest contact electrode. This time lag will depend on the reactivity parameter of the device, given by,

$$\chi^2 = \rho(g + i\omega c),\tag{1}$$

where $\rho$ is the sheet resistance of the high resistance electrode, $c$ and $g$ denote the capacitance and conductance of the LC layer per unit area respectively, and $\omega = 2\pi f$ is the angular frequency of the applied voltage. The precise voltage distribution over the corrector aperture could be obtained by solving the equation that follows from Kirchoff's law for the electric analogue of a modal LC corrector,

$$\nabla^2_{x,y} V = \chi^2 V \,.\tag{2}$$

Here $V$ is the amplitude of the applied voltage. The solution to this equation is considered in Ref. [16] and, in the case that just the central electrode is connected, is given by,

$$V(r) = V \frac{N_1(i\chi l)J_0(i\chi r) - J_1(i\chi l)N_0(i\chi r)}{N_1(i\chi l)J_0(i\chi a) - J_1(i\chi l)N_0(i\chi a)},\tag{3}$$

where $J_n$ and $N_n$ (n = 0, 1) are the Bessel functions of the first and second kinds [20] ($n$ is the order of each) respectively, $a$ is the contact electrode radius, and $l$ is the aperture radius. The calculations assumes that the LC molecules are completely aligned with the electrical field and the sheet capacitance and conductance of the LC layer are equal to,

$$c = \frac{\varepsilon_0 \varepsilon'_\parallel}{d}, \qquad g = \frac{\varepsilon_0 \varepsilon''_\parallel \omega}{d},\tag{4}$$

where $\varepsilon_0$ is the permittivity of free space, $\varepsilon'_\parallel$ and $\varepsilon''_\parallel$ are the real and imaginary parts of the dielectric constant of the LC layer measured along the director axis (in this particular case, $\varepsilon'_\parallel$=18, $\varepsilon''_\parallel$=1.4), and $d$ is the thickness of LC layer. For partial alignment of the LC molecules $c$ and $g$ are calculated from more precise formulas, given in the Ref. [19].
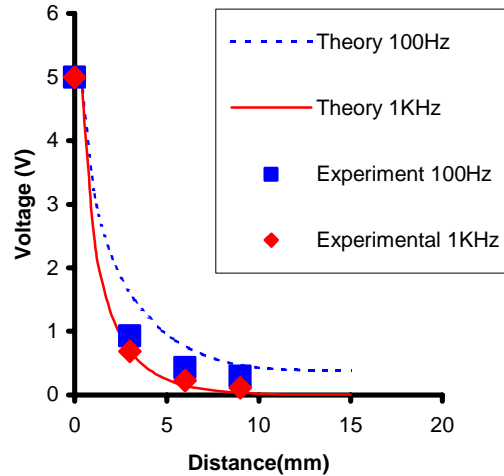


Fig 2. Experimental and theoretical curves for the dependence of the rms voltage across the cell versus the distance from the contact, for an applied voltage of 5V. The lines show the theoretical results (continuous = 100 Hz, and dashed = 1KHz) and the points show the experimental points for 100 Hz (squares) and 1Khz (diamonds).

The calculated amplitude distribution $V(r)$ was compared with an experiment. Just one electrode was connected to a signal generator, and the others were left floating. The voltages at the other electrodes were measured with a voltmeter in order to give $V(r)$ at a number of discrete points. The measurements of the electric field distribution were performed using frequencies ranging from 40 Hz to 5 kHz and the calculated and experimental curves are shown in Fig. 2. for the central electrode voltage of 5 V for 100 Hz and 1 kHz. There is sufficient agreement between theory and experiment for the theory to be useful when controlling the device. In general, the $V(r)$ curve becomes steeper with increasing frequency, and the influence function is more tightly restricted around the region of the contacts, caused by an increase of $\chi^2$. Because the phase shift in the LC is a non-linear function of voltage, then the difference in the phase response between high and low frequencies is more distinct than Fig. 2 implies. Strictly speaking, the shape of the influence function is different for different control contacts across the aperture.

## 3. Influence function characteristics

To study the corrector characteristics the apparatus shown in Fig. 3 was used. The corrector was aligned with a polarizer oriented at 45° to the LC axes in order to visualise the phase modulation. The laser beam passes through the LC layer and is reflected from the dielectric mirror. Then it passes through the LC layer again. The polarizer produces an intensity modulation: $I \sim \sin^2(\Delta\phi(r))$, where $\phi(r)$ is the measured phase retardance distribution. The amplitude-modulated laser beam is focused by lens *2* on to the photo-diode. The photo

current is amplified and measured by the digital oscilloscope. To make spatial measurements of the $\Delta\Phi(r)$ distribution the photo diode was replaced by the CCD-camera with the additional lens *3*. The camera and the lens *3* are shown in Fig. 3 by the dashed-line inset.
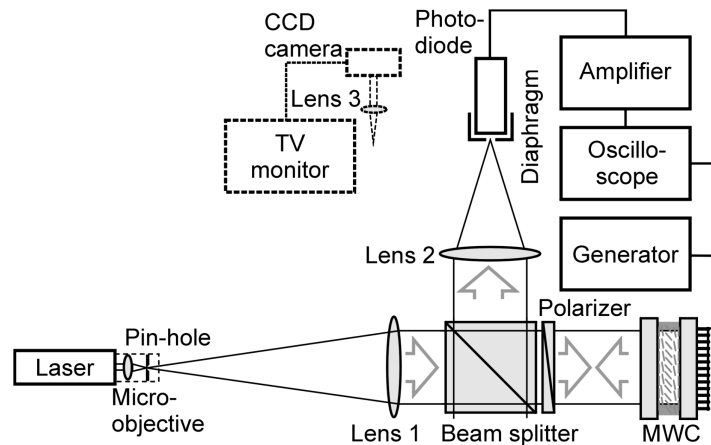


Fig 3. Experimental apparatus for measuring the optical characteristics of the LC-MWC. In the setup shown, the apparatus can be used to measure the global properties (such as voltage-phase response, and switching times). Lens 2, the diaphragm, and the photodiode are replaced with the inset apparatus (lens 3, CCD and monitor) to image the device.

Figure 4 shows interferograms obtained for square wave voltages with 100 Hz frequency and amplitudes of 4 V (Fig. 4a) and 10 V (Fig. 4b), and indicates how the influence function changes with voltage. In Fig. 4c the amplitude of the voltage was kept the same as in 4b. but the frequency increased to 10241Hz, showing the decrease in width. In general, the width of the optical response increases with voltage and decreases with frequency. Only one contact was electrically connected, and thus the influence function can extend beyond the neighbouring contacts, as shown in Fig. 4b If the surrounding contacts are grounded the influence function is narrower although it still depends on both voltage and frequency. The curves of half-width response versus frequency and voltage are plotted in Fig. 5 for both cases of earthed and floating neighbouring contacts.
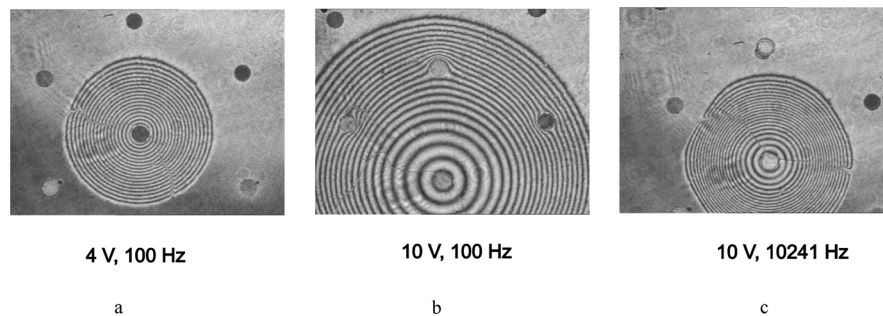


4 V, 100 Hz        10 V, 100 Hz        10 V, 10241 Hz

a        b        c

Fig. 4. The central part of the LC-MWC showing how the influence function varies with both the amplitude and frequency of the voltage. a) $V=4$V, $f=100$ Hz; b) $V=10$V, $f=100$ Hz; c) $V=10$V, $f=10241$Hz. The other contacts are not earthed. N.B. The field of view of each photo is slightly different, but the spacing between the contacts can be used as a measure of scale.
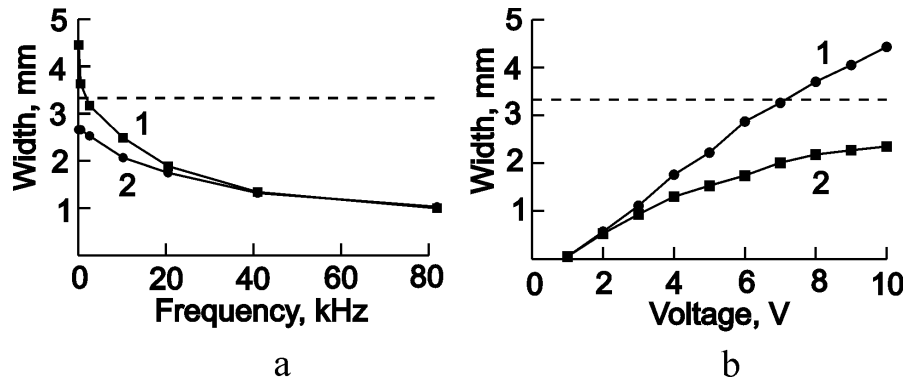
Fig. 5. Half-widths of the influence function versus (a) frequency and (b) voltage. Curve 1 corresponds to the case when the adjacent contacts are not connected, and curve 2 – when they are grounded. The horizontal dotted line shows the spacing between contacts.
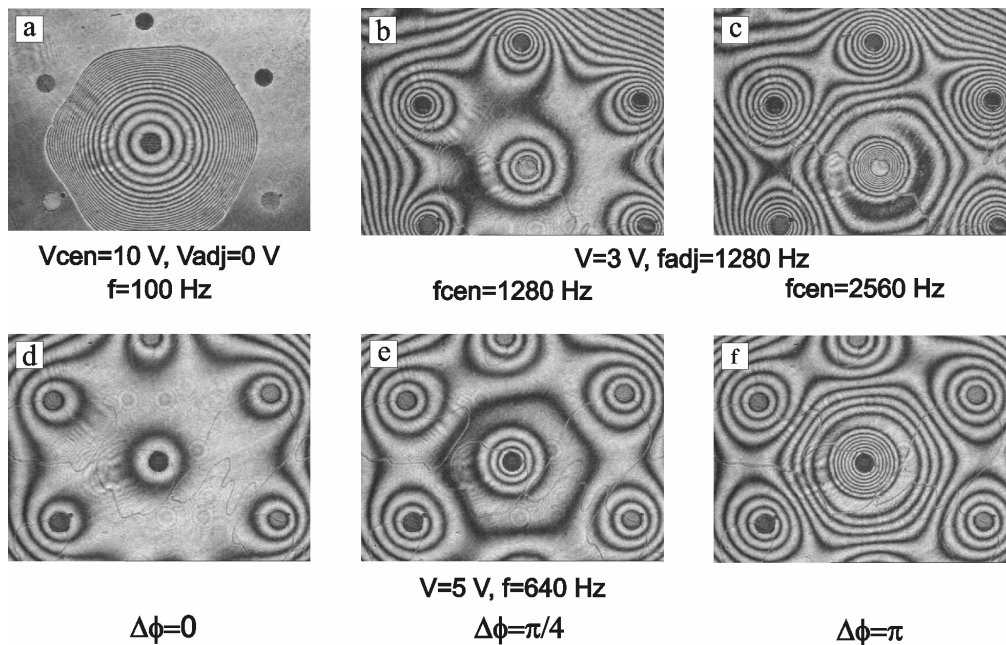


Fig. 6. Polarization interferograms for the central part of the LC-MWC for different applied control signals. *fcen* = frequency on central electrode. *fadj* = frequency on the electrodes adjacent to the central electrode.

Now consider the effect if voltages are applied to adjacent electrodes. First we note that there are two influence functions of interest. The first is the influence function around a contact of the electric field across the LC layer, and the second is the influence function of the phase shift induced by the LC layer (furthermore, the influence functions also change depending on whether the neighbouring electrodes are connected or not). The voltage across the LC layer at any point in the device is a linear superposition of the electric field influence functions (assuming that the influence functions when the surrounding electrodes are connected are used). However, the resulting phase response across the cell is not a linear combination of the individual phase influence functions because the LC voltage phase

relationship is non-linear. The voltage distribution and, correspondingly, the optical response of the corrector will be determined by the contacts layout, and the amplitude, frequency and phase of the voltage applied to the contacts. It should be noted that there is no general analytical solution of this problem. The voltage distribution in the LC layer can be calculated using a numerical model, as described later.
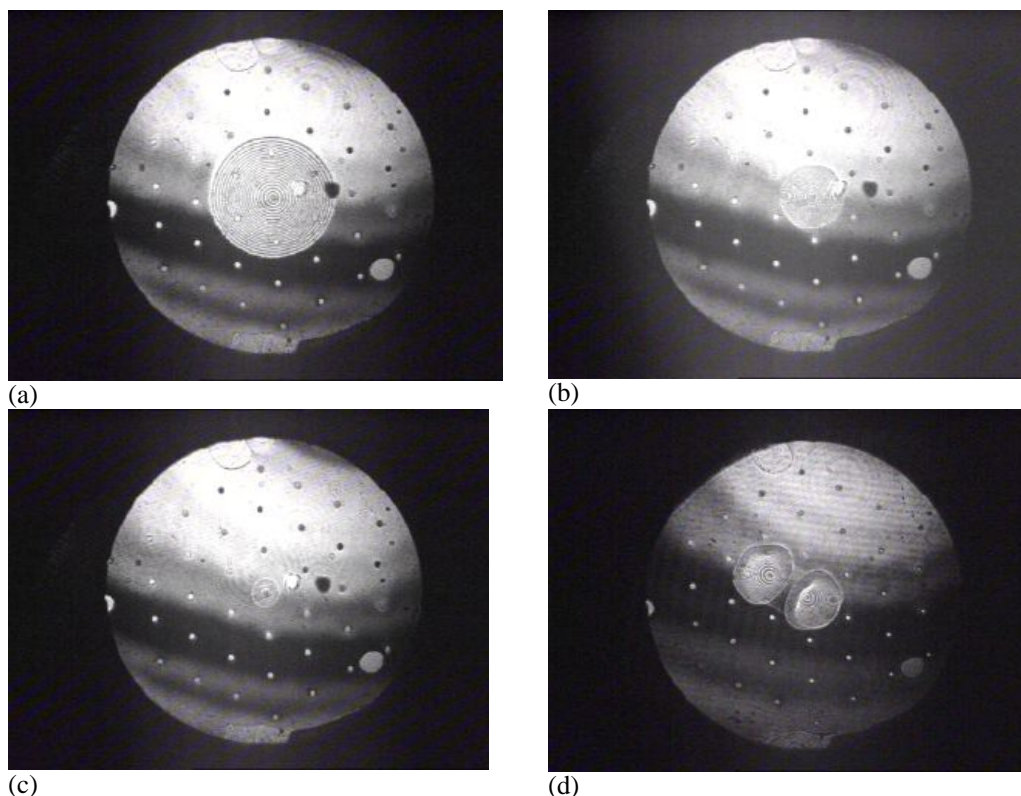


(a)

(b)

(c)

(d)

Fig. 7. Movies showing how the voltage applied to the contacts affects the influence functions. In 7a. (547 KB) the voltage is increased from 0 to 20V on the central electrode at a frequency of 20Hz. The other contacts are not earthed. 7b (547 KB) is identical except that the surrounding electrodes are earthed. In 7c. (412 KB) the voltage is fixed at 20V and the frequency varies from 50 Hz to 90KHz (the other connections are earthed). A 20V 50Hz voltage is applied to two adjacent contacts in 7d (447 KB) and the relative phase is varied from 0 to π. The dark band across the whole field is due to a non-uniform LC layer. Some further blemishes in the cell can be seen as dark marks. The fringes are not distinct because of losses due to file compression.

The dependence of the influence functions on the neighbouring electrodes is shown in Fig. 6a, for a 10 V, 100 Hz signal applied to the central contact and the adjacent contacts are grounded (compare with Fig. 4b in which case the other contacts are floating). The influence of the adjacent contacts is shown in Fig. 6b and c. The central contact and the adjacent six are supplied with a 3 V voltage. The frequency of the adjacent contacts was kept fixed at 1280 Hz, and for the central contact was varied: 1280 Hz (Fig. 6b) and 2560 Hz (Fig. 6c). This is an example of so-called "incoherent" composition of influence functions, when different contacts are driven by AC voltages having different frequencies. Further studies of the LC-MWC will investigate this mode of operation.

The influence of the phase difference of the controlling voltage of adjacent electrodes manifests equally clearly. The interferograms shown in Fig. 6d,e, and f correspond to different phase delay values of the central contact voltage with respect to the neighbouring contacts. A voltage of 5V 640 Hz was used and the phase was varied as indicated in the figure. When there is no phase difference, the resulting voltage distribution is approximately constant between the contacts, and the optical phase response is approximately uniform (Fig. 6d) with small phase-bumps around the control contacts. We will discuss appearance and removing of these bumps in section 5. In part f. when there is a phase difference of $\pi$, then at any instant of time, the voltage varies from +V (or –V) at the central contact to –V (or +V) at any of the neighbouring contacts. There is therefore a voltage slope of height 2V. The LC, however, responds to the rms voltage which therefore varies from V at the contacts to 0 halfway between them. The resulting sharp change in phase response is shown in part f. Using a deformable mirror, with the 7 actuators arranged in a similar arrangement to that in Fig.1b, it would be impossible to switch from the phase profiles shown in parts d. and f. Results shown in part e. show an intermediate effect when the phase different is $\pi/4$.

The effect of the voltage amplitude, frequency, and phase can also be seen in the movies, in Fig. 7.
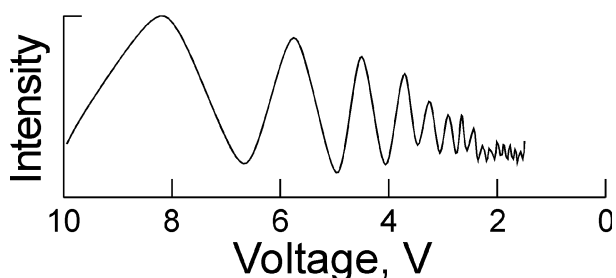
## 4. Voltage-phase calibration

Fig. 8. Total intensity modulation of reflected laser beam from LC-MWC, obtained by means of polarizer.

In order to accurately control the LC-MWC it is necessary to determine the voltage-phase characteristics. The structure of the LC-MWC means that these are slightly different from a normal LC cell with low resistance electrodes, and therefore the characteristics must be calibrated using the actual LC-MWC. The experimental apparatus in Fig. 3 was used with the pinhole in order to collect light from the whole device. The integrated intensity modulation versus voltage (100 Hz) is shown in Fig. 8. The broad influence functions for low frequencies means that at high voltages, the intensity is approximately uniform across the cell. Therefore, as the voltage varies the integrated signal across the cell varies by a large amount. However, at lower voltages, where the phase varies more sharply with voltage, then the intensity varies across the device and therefore there is little change in the signal versus voltage as shown Fig. 9.
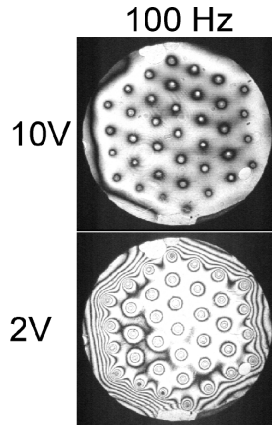
100 Hz

10V

2V

Fig. 9. The LC-MWC with a constant voltage and frequency being applied to all the contacts: top –10V, bottom – 2V. The voltage varies by a small amount in between the control contacts, but because the voltage-phase response is non-linear (with the highest sensitivity at low voltages) then the phase varies across the device for low voltages, as shown.

These data were used to plot a standard curve $\Delta\Phi(V)$, shown in Fig. 10 by solid line 1. This curve has been extrapolated for low voltages by a dashed line. Visual observations showed that the threshold voltage is close to the extrapolated value of 1.23 V. For comparison, Fig. 10 also shows the voltage phase characteristics of the LC material. The threshold voltage of LC-MWC is higher than the threshold voltage for an ordinary cell of the same LC material. The reason is the voltage drop across the high-resistance electrode.
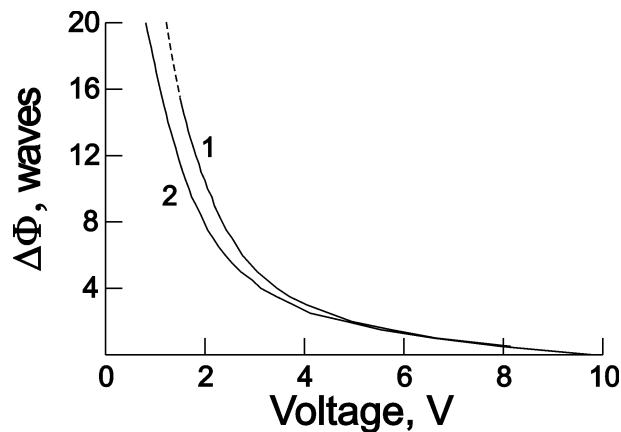


Fig. 10. Voltage-phase shift dependencies for LC-MWC (1) and for LC material (2).

## 5. Numerical model & low order aberration generation

A numerical model of the LC-MWC was developed for the case when all the contacts are controlled by AC voltages of the same frequency but different amplitudes. The analysis is based on the numerical solution of Eq. (2) with the boundary conditions for point-like contacts given in the form:

$$V\big|_{\sqrt{(x-x_k)^2+(y-y_k)^2}\le a/2}=V_k,\ k=1..37,\tag{5}$$

where $x_k$ and $y_k$ are coordinates of the $k$-th contact, $a$ is its diameter, and $V_k$ is the contact voltage. The absence of current flow through the edge of the aperture defines the boundary conditions,

$$y\frac{\partial V}{\partial x}+x\frac{\partial V}{\partial y}=0.\tag{6}$$

The voltage distribution in the LC-MWC is given in the form of a matrix where its real and imaginary parts $u_{ij}$ and $v_{ij}$ ($V_{ij}=u_{ij}+iv_{ij}$) are defined on a rectangular mesh with a spacing $h_x$ for the x-axis and $h_y$ for the y-axis, where $i=1..N_x$ and $j=1..N_y$ are the indices of x and y coordinates, correspondingly. The derivatives $\partial^2 V/\partial x^2$ and $\partial^2 V/\partial y^2$ in Eq. (2) are replaced with finite differences. After separation of real and imaginary parts it leads to linear expressions linking the voltage values at the adjacent points:

$$\begin{cases}\dfrac{u_{i-1,j}-2u_{ij}+u_{i+1,j}}{h_x^2}+\dfrac{u_{i,j-1}-2u_{ij}+u_{i,j+1}}{h_y^2}=\rho(gu_{ij}+\omega cv_{ij})\\[4mm]\dfrac{v_{i-1,j}-2v_{ij}+v_{i+1,j}}{h_x^2}+\dfrac{v_{i,j-1}-2v_{ij}+v_{i,j+1}}{h_y^2}=\rho(gv_{ij}-\omega cu_{ij})\end{cases}.\tag{7}$$

A direct solution of system (7) requires the storage of huge arrays in memory as the dimension of the main matrix is of size $N_x N_y \times N_x N_y$, and therefore an iterative solution was used. The unknown $u_{ij}$ and $v_{ij}$ in (7) can be expressed in terms of the voltage values at the adjacent points, and then sequentially calculated. The accuracy achieved at each step can be evaluated by using the Lipshitz condition [21],

$$\Delta=\frac{\delta_1^2}{\delta_0-\delta_1},\tag{8}$$

where $\delta_1$ is the maximum change of the voltage for the latest iteration step, and $\delta_0$ - for the previous one. The linearity of Eq. (2) means that it is possible to represent the solution as a sum:

$$V(x,y)=\sum_{k=1}^{37}V_k\varphi_k(x,y),\tag{9}$$

where $\varphi_k(x,y)$ is a set of solutions of equation (2) obtained with the following boundary conditions

$$\varphi_k(x_i,y_i)=\begin{cases}1,i=k,\\0,i\ne k,\end{cases}\tag{10}$$

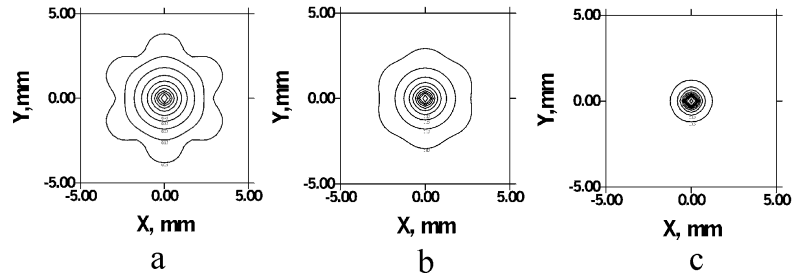These functions are response functions of the LC-MWC for a single-frequency control mode.

Fig. 11. Theoretical voltage response functions of the LC-MWC for a single-frequency control voltage: (a) f=40 Hz; (b) 10 kHz; (c) 100 kHz; the results are obtained by numerical simulation.

The voltage response function of the central contact for three different frequency values is shown in Fig. 11. Calculation parameters correspond to the parameters of the prototype: the sheet resistance of the control electrode is 6.78 MΩ/square, the diameter of the contact electrodes is 0.5 mm, the spacing between the contacts is 3.33 mm, the total corrector diameter is 30 mm, the specific LC layer capacity $c = 3 \cdot 10^{-12}$ F/mm$^2$, the specific LC conductance per unit area is $g = 2 \cdot 10^{-9}$ Ω$^{-1}$m$^{-2}$ for low frequencies. As is evident in Fig. 11. the response function is localized in the space limited by the neighbouring contacts, which is caused by the boundary conditions (Eq. 10). The width of the influence function reduces with frequency from the distance between contacts, to the contact diameter.

Next, the model was compared with theory by using the model to calculate appropriate voltages to be sent to the contacts in order to generate a specific phase distribution, which was then measured using the equipment in Fig. 3. The measured interference pattern was processed using "Quick Fringe" software [22]. The calibration curve 1 in Fig. 10 was used. Fig. 12 shows two parabolic phase profiles with different signs. The peak-to-value phase modulation over the active area was 4λ for $\lambda = 0.633$ μm. For viewing clarity, the phase profiles in Figs. 12a and 12b were inverted. The RMS deviation of the simulation results from an ideal parabolic phase profile was 0.0699 and 0.0406 for a positive and negative parabola, respectively. The corresponding experimental deviations were 0.4024 and 0.2247 waves.

It can be seen that the localization of the theoretical response functions results in non-homogeneities of the resulting wave front, visible as "phase-bumps" (see Fig. 6, Section 3.) around the contacts. The lack of these bumps in the experimental results shown in Fig. 12b and 12d is because the software "Quick Fringe" only used 36 Zernike polynomials, and thus the very high spatial frequencies are filtered out. We observed the high frequency spatial modulation on contact locations in the experimental interferograms.

Finally we generated the first five Zernike modes: tilt, defocus, astigmatism, coma and spherical aberration. These were quality results, which were obtained by proper manual selection of control voltages. The results were monitored in ZYGO interferometer. Phase profiles and isophase lines for the mentioned aberrations are shown in Fig. 13.
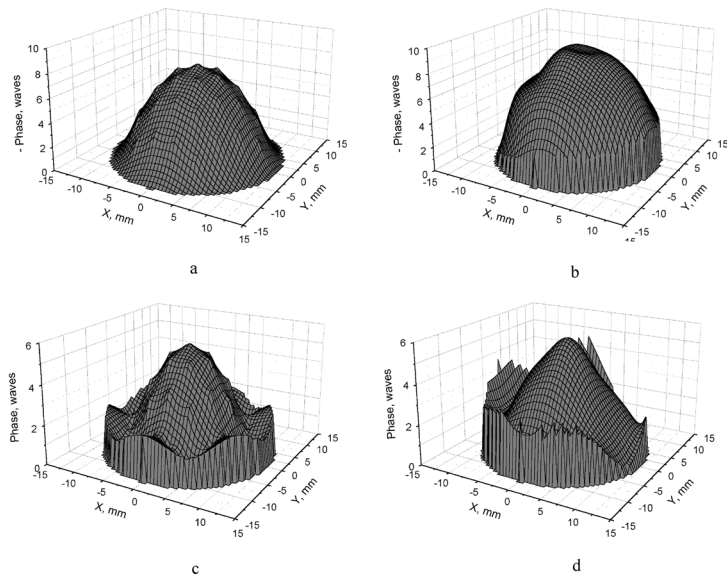
Fig. 12.  Comparison of calculated and experimental phase distributions for 37-contact MCC prototype with hexagonal arrangement of contacts: (a) parabola with positive sign, numerical simulation; b) parabola with positive sign, experiment; (c) parabola with negative sign, numerical simulation; d) parabola with negative sign, experiment.
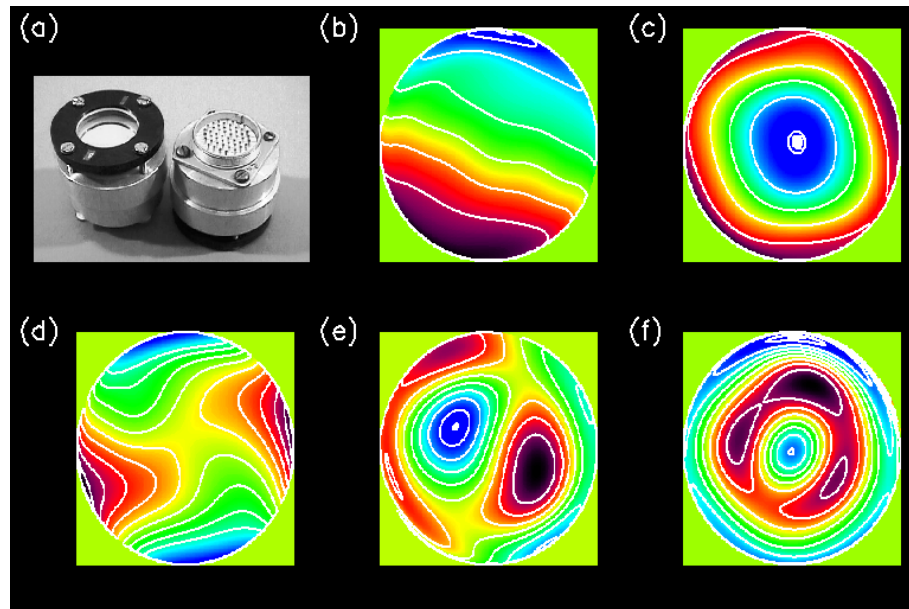


Fig. 13. (a) A photo front a rear connectors of a 33mm aperture device. (b)-(f) Qualitative generation of low order Zernike modes: (b) tilt, (c) defocus, (d) astigmatism, (e) coma and (f) spherical aberration. The contour lines are drawn at half-wave intervals ($\lambda$=0.633µm).

## 6. Constructional Details and Control of the Wavefront Corrector

The LC-MWCs were produced using a 25μm thick layer of liquid crystal. The deposited alignment layer was a rubbed polyimide coating (ZLI-2650, Merck, Germany). The main criterion for the choice of LC material was high optical anisotropy. E49 LC material (Merck, Germany) was used which has a birefringence $\Delta n = 0.26$. The low resistance electrode was a conventional ITO (indium tin oxide) with a resistance of 200 Ω/square. The main challenges in producing the devices were the production of the high resistance electrodes and the construction of the back-substrates with point contacts running through them. The latter were made in the following manner. Both the substrate glass and the wire contained molybdenum as an additive which meant that their expansion coefficients were closely matched. An array of contact electrodes was arranged in a graphite jig and placed below the substrate glass. The glass was heated until it was soft so the contacts could be pushed through the glass. Care was taken to ensure that the electrodes didn't oxidise and that micro-bubbles didn't form in the substrate. The device was then annealed and polished. A dielectric mirror deposited onto a high-resistive electrode consisted of 21 layers and was optimised for a wavelength of 632.8 nm. A photo of the device is shown as an insert in Fig. 13
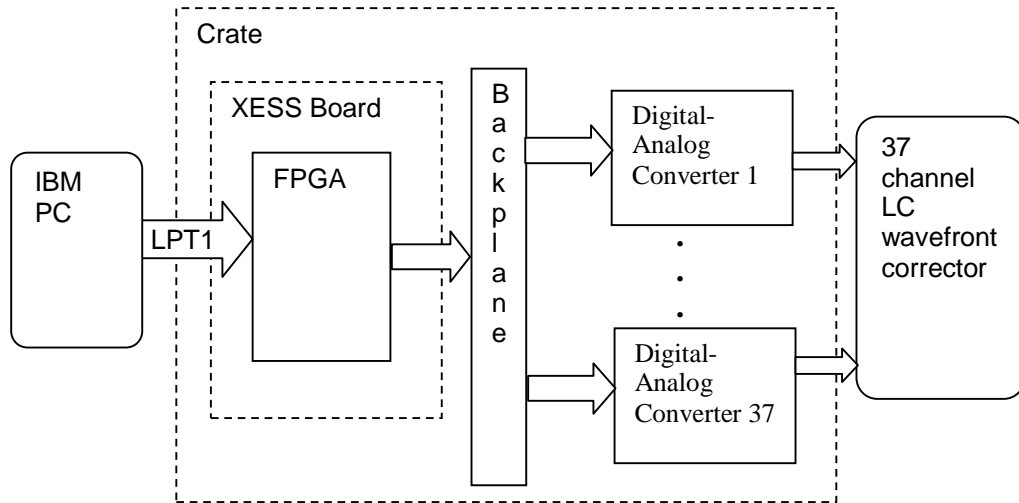
Fig. 14. Block diagram of the FPGA control unit.

A control system was produced to simultaneously drive all the 37 channels of the LC-MWC with square wave signals, allowing independent control of the voltage, frequency, phase and mark to space ratio of each channel. The block diagram of the control unit is shown in Fig. 14. The key to the control system is a Xilinx [24] Field Programmable Gate Array (FPGA), the XCV100. The FPGA is mounted on a XESS [25] evaluation board, which provides the power regulation, programming and clock signals required by the FPGA. The main reason for choosing this type of system is that the AC signals used to drive the LC-MWC are all generated using the FPGA whereas the relatively slowly varying control signals (i.e. the signals controlling the amplitude, frequency etc) are produced by the computer.

The control logic implemented in the FPGA receives and stores data defining the parameters for each output channel from the PC via the parallel port, and uses this to generate

the waveforms via the DAC cards. We used two 32 channel DAC cards. The DAC and amplifier chips cover an output range of –10 V to +10 V, with a resolution of 2.44 mV. The entire system is contained in a crate.

## 7. Conclusions

The paper contains the description of a manufacturing technology for modal LC-correctors as well as the results of the research of a particular one of them, a 37-channel corrector with a 30-mm aperture. The optical response of the corrector as the function of amplitude and frequency of the voltage supplied has been investigated both experimentally and by means of a numerical model.

The results confirm a strong dependence of the optical response on the amplitude and frequency of the applied voltages, and on the arrangement of nearby contacts. An experimental demonstration of creating different wave front modes described by the first few Zernike polynomials was shown.

A new 70 mm device with an additional annular 38th control contact is shown in Fig. 15. The next generation of modal LC-correctors will be based on silicon technology [26]. The silicon-based corrector will use a silicon plate, which already has the distributed resistance easy matching to electrical properties of LC by an alloying addition. The contact addressing will be performed by a lithography technique.



Fig. 15. A larger aperture (70mm) liquid crystal modal wavefront corrector (the battery is shown for scale).